Coupled Personalisation of Cardiac Electrophysiology Models for Prediction of Ischemic Ventricular Tachycardia

Jatin Relan, Phani Chinchapatnam, Maxime Sermesant*, Kawal Rhode, Matt Ginks, Hervé Delingette, C. Aldo Rinaldi, Reza Razavi, Nicholas Ayache

***Abstract*—In order to translate the important progress in cardiac electrophysiology modelling of the last decades into clinical applications, there is a requirement to make macroscopic models that can be used for the planning and performance of the clinical procedures. This requires model personalisation i.e. estimation of patient-specific model parameters and computations compatible with clinical constraints. Simplified macroscopic models can allow a rapid estimation of the tissue conductivity, but are often unreliable to predict arrhythmias. Conversely, complex biophysical models are more complete and have mechanisms of arrhythmogenesis and arrhythmia-sustainibility, but are computationally expensive and their predictions at the organ scale still ha to be validated. We present a coupled personalisation framework which combines the power of the two kinds of models while keeping the computational complexity tractable. A simple Eikonal (EK) model is used to estimate the conductivity parameters, which are then used to set the parameters of a biophysical model, the Mitchell-Schaeffer (MS) model. Additional parameters related to Action Potential Duration (APD) restitution curves for the tissue are further estimated for the MS model. This framework is applied to a clinical dataset derived from a hybrid XMR imaging and non-contact mapping procedure on a patient with heart failure. This personalised MS Model is then used to perform an *in silico* simulation of a Ventricular Tachycardia (VT) stimulation protocol to predict the induction of VT. This proof of concept opens up possibilities of using VT induction modelling in order to both assess the risk of VT for a given patient and also to plan a potential subsequent radiofrequency ablation strategy to treat VT.**

I. Introduction

Cardiac arrhythmias including ventricular tachycardia are increasingly being treated by Radio-Frequency (RF) ablation. These procedures can be very effective but still have unsatisfactory success rates widely ranging from 50−90%, with a 20−40% late recurrence rate, due to a lack of clinical consensus on the optimum RF ablation strategy [1]. There is a need for substantial guidance in locating the optimum ablation strategy [2].

This guidance could be provided by personalised *in silico* cardiac electrophysiology models, as such models may allow different ablation strategies to be tested. A personalised model incorporates estimation of patient-specific parameters which best fit the clinical data. Such a step is necessary to reveal hidden properties of the tissue that are used to predict the behaviour under different pacing conditions.

There is a large variety of cardiac electrophysiology models for myocyte action potential developed at cellular and sub-cellular scales [3], [4], [5], [6], [7]. Cardiac tissue and whole-heart electrophysiological computations of these models are based on the principles of reaction-diffusion systems [8], [9]. According to the reaction term computation, these models can be broadly categorised as Biophysical Models (BM), Phenomenological Models (PM) and Generic Models (GM). BM [5], [6] model ionic currents and are the most complete and complex but are less suitable for parameter estimation from clinical data due to a high computational cost and to the lack of observability of their parameters. PM [10], [11] are based on PDEs and are of intermediate complexity level and less computationally expensive. GM [12], [13] represent simplified action potentials and are the least complex. Simple Eikonal Models (EM) [14], [15], [16] model the action potential propagation in the cardiac tissue without modelling the action potential itself. They can be very fast to compute [17], but less reliable in arrhythmia predictions due to the complexity of both the refractoriness and the curvature of the wavefront.

Computational modelling of cardiac arrhythmogenesis and arrhythmia maintenance using such models has made a significant contribution to the understanding of the underlying mechanisms [18], [19], [20], [21], [22], [23]. These studies have shown a host of factors involved in the onset of arrhythmia with wave fragmentation and spiral wave breakups, which include realistic ventricular geometry [24], heterogeneity in repolarisation [25] and APD restitution [26], [27] and CV restitution [28]. A combined clinical study and synthetic modelling of APD restitution was shown in [29]. In this paper, we study these properties for a clinical dataset and evaluate its role in ischemic Ventricular Tachycardia (VT) induction.

To introduce models directly into clinical practice, the ideal requirements are low computational complexity, fast estimation of parameters (quick personalisation) and reliable predictions. These attributes cannot be found in one single model, thus here we present a novel approach, wherein we combine two models to obtain these attributes and apply them to a clinical dataset. We use a coupled personalisation framework, which is fast and combines the benefits of an Eikonal (EK) model [30] with those of a simplified biophysical model, the Mitchell-Schaeffer (MS) model [31]. The fast 3D EK model is used to estimate

* *corresponding author - email: maxime.sermesant@inria.fr*

J. Relan, M. Sermesant, H. Delingette and N. Ayache are with INRIA, Asclepios research project, Sophia Antipolis, France

K. Rhode, M. Ginks, C.A. Rinaldi, M. Sermesant, P. Chinchapatnam and R. Razavi are with the King's College London, Division of Imaging Sciences, St. Thomas Hospital, United Kingdom.

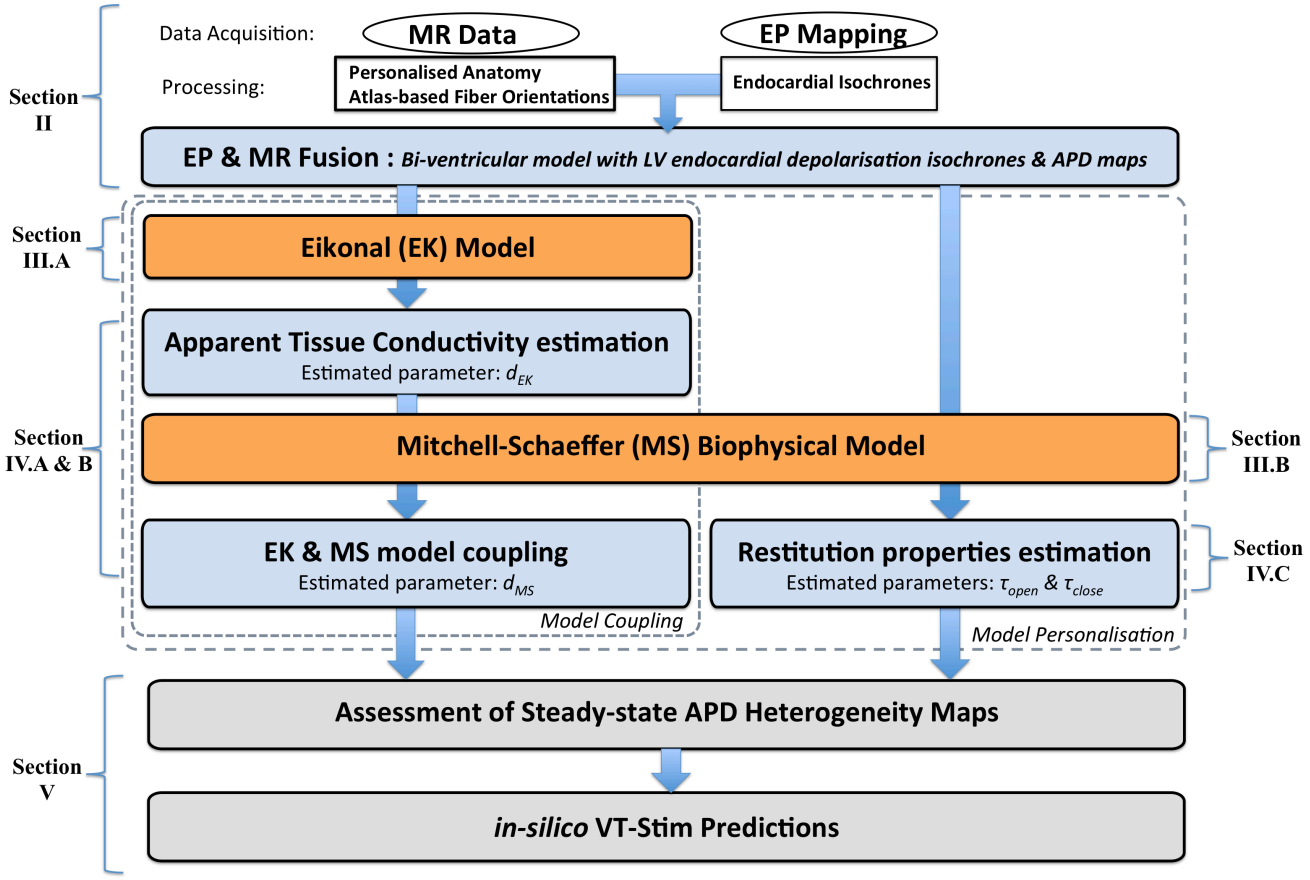

Fig. 1. Flowchart describing the outline of this paper.

the tissue conductivity parameter over the ventricles derived from non-contact mapping of the endocardial surface potential, using an adaptive iterative algorithm. This is then used to set the conductivity parameter of the 3D MS model. Additional parameters related to APD restitution properties of the tissue are then estimated locally using directly the 3D MS model and the measured endocardial surface potential.

This framework is applied to a clinical dataset from a patient with heart failure and myocardial scar on MRI scanning using electrophysiological data from a non-contact mapping study performed in a hybrid X-ray/magnetic resonance (XMR) suite [32]. The ventricles were mapped with a statistical atlas for cardiac fibres [33](Fig. 2). The resulting personalised 3D MS model is then used to simulate a clinical VT-Stimulation (VT-Stim) procedure to show a potential application of VT induction modelling. Fig. 1 shows the framework of the coupled personalisation method and VT induction modelling, used in this paper.

II. Clinical Context

In order to evaluate the inducibility of VT in patients, the clinical procedure involves stimulation with an EP catheter usually in the RV apex at different cycle lengths. This type of protocol is used to test if re-entrant VT can be induced by such pacing in patients at risk of VT. Such studies may be useful in predicting the risk of VT for an individual patient but provide limited information on which to base a potential ablation strategy of re-entrant VT circuits.

Our aim is to create a personalised electrophysiological model of a given patient to which a virtual VT stimulation procedure can be applied. Moreover, a virtual RF ablation procedure can then be applied to the model in order to test potential ablation strategies.

In order to validate this approach, we have used an extensive clinical dataset, derived from mapping of the LV endocardium. Such mapping is not routinely performed for a VT-Stim procedure, however it is sometimes used to guide RF ablation. This clinical dataset was obtained from an electrophysiology study performed in a hybrid X-ray/MR environment. The electrical measurements obtained using an Ensite system (St Jude Medical) were registered to the patient anatomy using XMR registration [32] (Fig. 4b).

A. Depolarisation and Repolarisation times extraction

The electrical data was collected with high pass filter settings for prominent QRS detection and with low pass filter for T-Wave detection.

The depolarisation times were detected within the QRS window set from surface ECG (Fig 3a) and were derived from the zero crossings of the Laplacian of the measured unipolar electrograms V (Fig. 3b & 6a). The surface Laplacian of electrograms gave reasonable results even in the

case of multiple deflections and also allows detection of local activation without interference from far-field activity [34].

The repolarisation times were detected within the ST window in surface ECG (Fig 3a) and were derived using the "alternative method" as compared to the standard wyatt method, because (*i*) most of the positive T-wave electrograms had an indiscernible steep upstroke for repolarisation time detection with wyatt method, (*ii*) a closer correlation was obtained between ARI and MAP duration with alternative method, as discussed in [26] and (*iii*) difference in APD extraction from the two methods had only a minimal influence on the restitution slopes and spatial distributions [29]. The measured T-wave polarity maps had positive T-waves for early repolarising sites and negative for late as in agreement to [35] (Fig. 4).

The alternative method has repolarisation times derived from dV/dt_{max} for the negative T-wave, at the dV/dt_{min} for the positive T-wave, and the mean time between dV/dt_{max} and dV/dt_{min} for the biphasic T-waves (Fig. 3c, 4, 5 & 6c).

The data was collected during intrinsic sinus rhythm and atrial pacing mode at 100 beats per minute (bpm), see Fig. 5. Myocardial scar was segmented manually from the Delayed Enhancement MR image.

The patient was a sixty year old woman with heart failure and NYHA class III symptoms. The patient had a dilated cardiomyopathy with sub-critical disease on coronary angiography although cardiac MRI showed subendocardial postero-lateral scar in the left ventricle. The left ventricular ejection fraction was 25% on maximal tolerated heart failure medication. The surface ECG demonstrated significant conduction disease with left bundle branch block (LBBB) and a QRS duration of 154 ms (normal QRS is less than 120 ms). Echocardiography, including Tissue Doppler, confirmed significant mechanical dysynchrony in keeping with the ECG findings.

This patient was selected for cardiac resynchronisation therapy (CRT). When implanting a CRT device, there is a choice between a standard device, or one also integrating a defibrillator. Therefore, evaluating the risks of VT in such CRT patients is important.

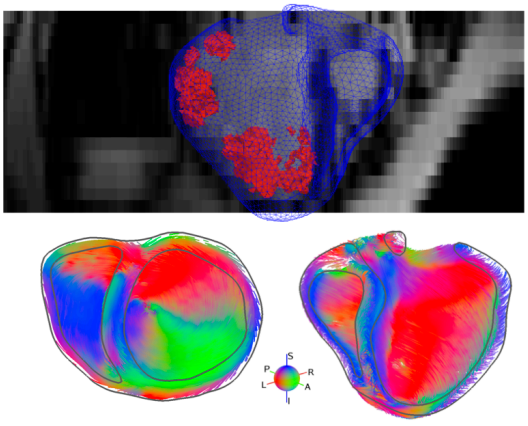

Fig. 2. Top: MR derived segmented mesh with scars (in red). Bottom: Fibre orientations based on a statistical atlas.

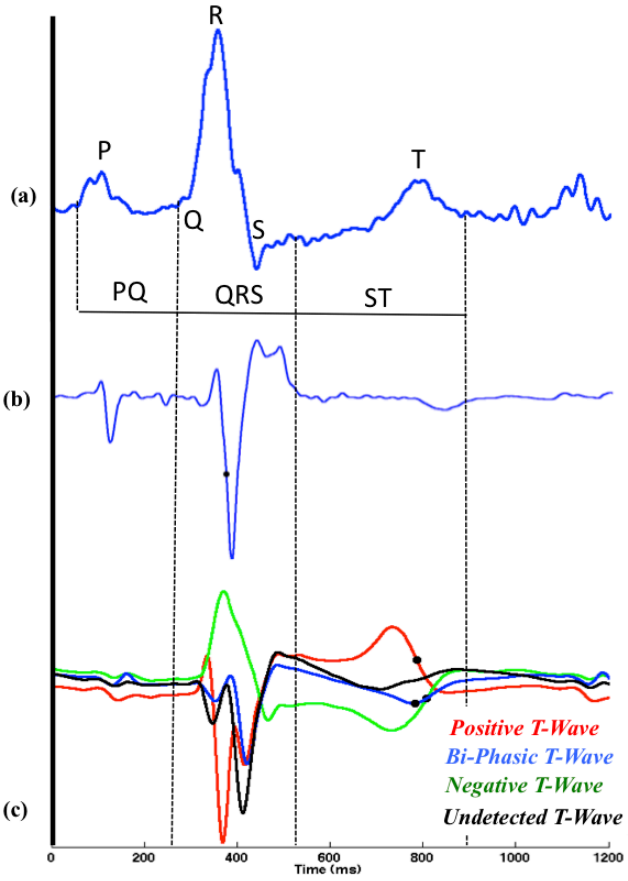

Fig. 3. (a) Measured surface ECG I, with QRS window (for depolarisation time extraction) and ST window (for repolarisation time extraction). Ensite surface unipolar electrograms (b) with high-frequency band-pass filter for detection (black dots) of depolarisation times, and (c) with low-frequency band-pass filter for detection repolarisation times, from positive(red), negative (green) and biphasic (blue) T-waves. Few electrograms had indiscernible T-waves (black).

III. Cardiac Electrophysiology Models

A. Eikonal Model (EK Model)

The EK model simulates the propagation of the depolarization wave in cardiac tissue, ignoring repolarisation phase. The EK model is governed by the eikonal-diffusion (ED) equation [36], [15] and is solved using the Fast Marching Method (FMM). It can be written as

$$c_0\sqrt{d_{EK}}\left(\sqrt{\nabla T(x)^t \mathbf{M} \nabla T(x)}\right) - \nabla\cdot(d_{EK}\mathbf{M}\nabla T(x)) = \tau(x) \quad (1)$$

where the superscript t denotes transpose, c_0 is a dimensionless constant ($= 2.5$), and $\tau(x)$ is the cell membrane time constant ($= 0.003\ s$). d_{EK} is the square of the tissue space constant along the fibre and is related to the specific conductivity of the tissue in the fibre direction, and has units of m^2. The anisotropy is incorporated in the diffusion tensor $\mathbf{M} = diag(1, \rho, \rho)$, with ρ the anisotropy ratio between longitudinal and transverse diffusion. We

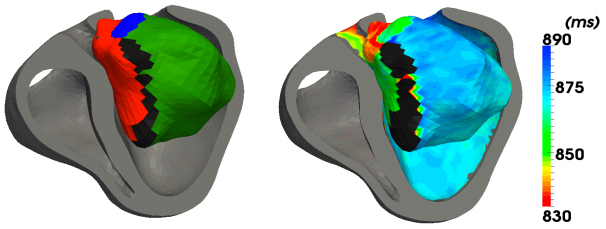

(a) T-Wave polarity (b) Isochrone projection

Fig. 4. (a) T-Wave polarity map on ensite LV surface, with positive (red), negative (green), bi-phasic (blue) and undetected (black) T-waves. (b) Repolarisation times projection from ensite LV surface to MR LV endocardium after XMR registration. Black: undetected repolarisation times.

use $\rho = 1/2.5^2$ in order to have Conduction Velocity (CV) 2.5 times faster in the fibre direction [14]. The non-linear Eq 1 is solved using a fixed point iterative method combined with a very fast eikonal solver as explained in details in [30], [17].

B. Simplified Biophysical Model (MS Model)

The MS model [31] is a 2-variable simplified biophysical model derived from the 3-variable Fenton Karma (FK) ionic model [37]. It models the transmembrane potential as the sum of a passive diffusive current and several active reactive currents including combination of all inward (primarily Na^+ & Ca^{2+}) and outward (primarily K^+) phenomenological ionic currents. The MS model is described by the following system of partial differential equations,

$$\begin{cases} \partial_t u &= div(d_{MS}\mathbf{M}\nabla u) + \frac{zu^2(1-u)}{\tau_{in}} - \frac{u}{\tau_{out}} + J_{stim}(t) \\ \partial_t z &= \begin{cases} \frac{(1-z)}{\tau_{open}} & if \quad u < u_{gate} \\ \frac{-z}{\tau_{close}} & if \quad u > u_{gate} \end{cases} \end{cases} \tag{2}$$

where, u is a normalised transmembrane potential variable, and z is a gating variable which makes the currents gate open and close, thus depicting the depolarisation and repolarisation phase. $J_{in} = (zu^2(1-u))/\tau_{in}$ represents the the inward currents which raises the action potential voltage and $J_{out} = -u/\tau_{out}$ represents the outward currents that decreases the action potential voltage describing repolarisation. J_{stim} is the stimulation current, at the pacing location. The literature values for reaction term parameters are given in [31]. τ_{in}, τ_{out}, τ_{open} and τ_{close} has units of s. The diffusion term in the model is also controlled by the diffusion tensor $\mathbf{M}$. In the longitudinal direction of the fibre, this pseudo-conductivity is set to d_{MS} which is one of the parameters we adjust, and to $d_{MS}.\rho$ in the transverse directions. d_{MS} has units of s^{-1}. The electrophysiology model is solved spatially using P1 Finite Element Method (FEM), and in time using an semi-implicit scheme as Modified Crank-Nicolson/Adams-Bashforth (MCNAB) scheme, which is evaluated in terms of accuracy, stability and computational time [38]. The parameter values and simulation details are given in Table. I & II

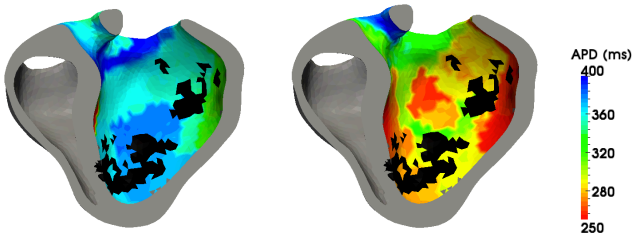

(a) Sinus rhythm (b) Paced mode

Fig. 5. Steady-state APD values measured from the Ensite data and projected on the LV surface, for (left) baseline and (right) pacing in the atria (at 100 bpm). Black represents scars.

Scars were modelled with zero conductivity in the ischemic zones. While the gray zones and the regions between scars (isthmus) had conductivity, APD RCs estimated from the data, as shown in Sec. V.A.

IV. Coupled Personalisation Method

A. Apparent Conductivity Parameter Estimation

Cardiac tissue conductivity is a crucial feature for the detection of conduction pathologies. The Apparent Conductivity (AC) of the tissue can be measured by the parameter d_{EK} in the EK model.

LV Endocardial values. AC is initially estimated on the endocardial surface as a global value using a simple bisection method which matches the average conduction velocity of the measured Depolarisation Time (DT) isochrones to the simulated ones. Using it as an initial guess, an adaptive multi-level domain decomposition algorithm is used, which minimizes the mean-squared difference of the simulated and measured DT isochrones at each level using a Brent's Optimisation Algorithm presented in [17]. Due to the absence of transmural electrical propagation information, we assume no variation across the left ventricle myocardium (excluding LV endocardium and scars) and hence we prescribe a single value for the myocardial tissue across the LV wall.

LV & RV Myocardial values. The AC values for RV endocardium and RV myocardial mass are set at 5.0 mm^2 and 0.64 mm^2 (from literature [14]). The LV myocardial AC value is estimated by one-dimensional minimisation of the following cost function (mean-squared difference of simulated and measured isochrones at endocardium + squared difference of simulated and measured QRS duration). The simulated QRS duration is calculated as the difference between the maximum and the minimum depolarisation times in the biventricular mesh and the measured QRS duration is estimated from the surface ECG.

B. Coupling of EK and MS Model Parameters

The AC parameter for EK model d_{EK} (Eq 1) is a scale for the diffusion speed of the depolarisation wavefront in the tissue. The model Conduction Velocity (CV) is related

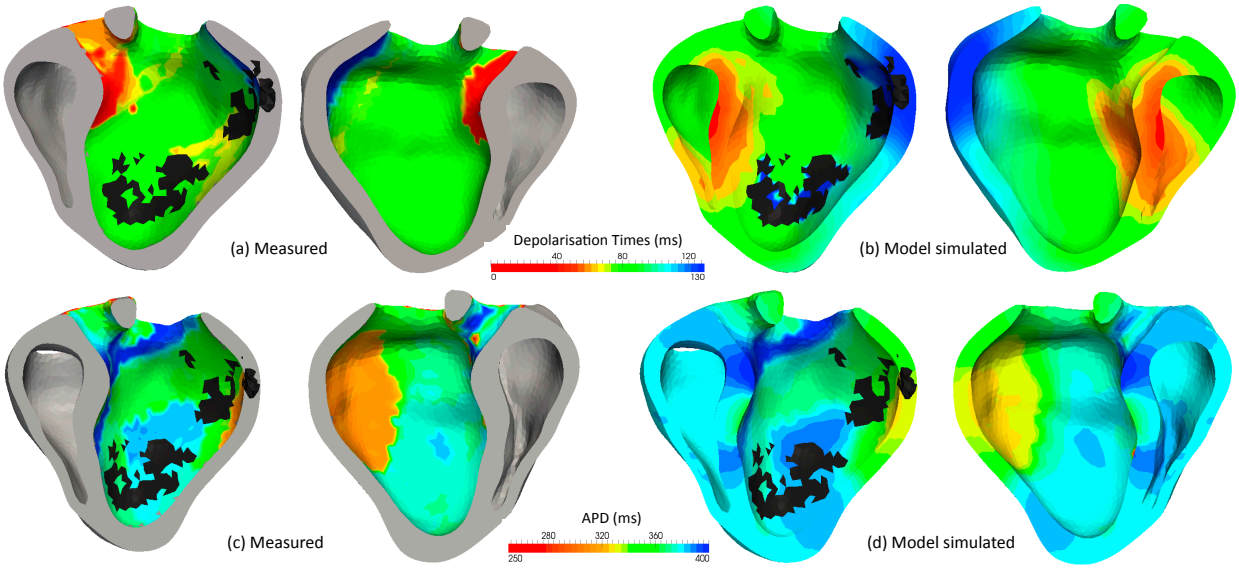

Fig. 6. Upper row shows the comparison of the measured Depolarisation Time (DT) isochrones on the LV surface only with model simulated DT isochrones on the whole heart, lower row shows the same for measured (LV surface only) and model simulated (whole heart) APD maps. Measurements are for baseline.

to d_{EK} (Fig. 7) as,

$$c_{EK} = \frac{c_0\sqrt{d_{EK}}}{\tau} \text{ in 1D } \& \; c_{EK} = \alpha_{EK}\sqrt{d_{EK}} + \beta_{EK} \text{ in 3D} \tag{3}$$

where the constants α_{EK} and β_{EK} are introduced to take into account the discretization errors (in particular of the curvature) in 3D.

The corresponding conductivity parameter for MS model, d_{MS} is also a scale for the wave diffusion speed in the tissue. The model CV here is related to d_{MS} (Fig. 7) as,

$$c_{MS} \propto \sqrt{\frac{d_{MS}}{\tau_{in}}} \text{ in 1D } \& \; c_{MS} = \alpha_{MS}\sqrt{d_{MS}} + \beta_{MS} \text{ in 3D} \tag{4}$$

where the constants α_{MS} and β_{MS} are introduced for the same reasons as of EK model, while τ_{in} is kept as a constant. The estimated AC parameter d_{EK} can then be used to estimate the parameter d_{MS}. The parameter d_{EK} gives model CV c_{EK}, which is similar to the actual measured data CV (c_{msd}) after the parameter estimation step. Thus to have MS model CV (c_{MS}) similar to the measured data, it has to be similar to EK model CV (c_{EK}). The constants α_{EK} and β_{EK} represent numerical curvature, diffusion and discretisation errors for EK model based on FMM. They are different from the constants α_{MS} and β_{MS}, which are diffusion and discretisation errors based on FEM. These constants are determined in 3D for the ventricular mesh. We performed several simulations with various d_{EK} and d_{MS} values and noted the corresponding c_{EK} and c_{MS} values. Then, we fit the analytical curves given in Eq 3 & 4 in least square sense and determine the constants. The constants estimated are $\alpha_{EK} = 802.25$, $\beta_{EK} = -268.54$, $\alpha_{MS} = 995.87$ and $\beta_{MS} = -554.38$. Thus from eq 3 & 4, we have $c_{EK} = 802.25\sqrt{d_{EK}} - 268.54$ and $c_{MS} = 995.87\sqrt{d_{MS}} - 554.38$. For a given CV, d_{MS} is slightly different from d_{EK}. This may be due to the fact that d has different units, as for EK model we model depolarisation time and for MS model we model transmembrane potential. However they both are scales for diffusion, thus such a coupling is performed. Then, the personalised d_{MS} values are computed from corresponding estimated d_{EK} values using 5 based on the condition, that $c_{msd} = CV = c_{EK} = c_{MS}$ after personalisation. Thus from eq 3 & 4, we have

$$d_{MS} = \left(\frac{\alpha_{EK}\sqrt{d_{EK}} + \beta_{EK} - \beta_{MS}}{\alpha_{MS}}\right)^2 \tag{5}$$

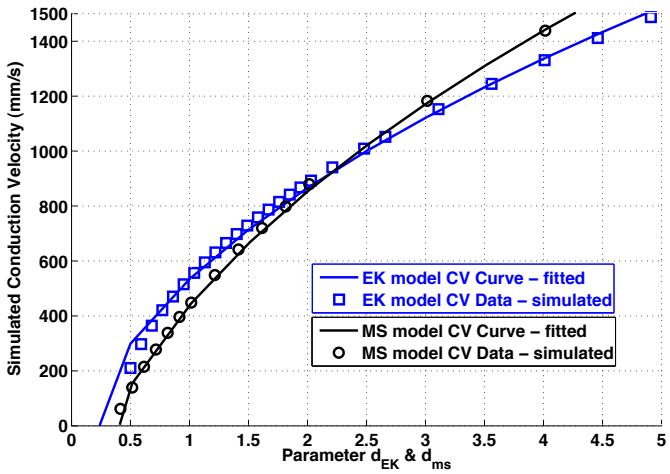

Fig. 7. Parameter d_{EK} and d_{MS} relationship with simulated conduction velocity CV for both models.

C. Parameter Estimation for APD Restitution

APD Restitution is an electrophysiological property of the cardiac tissue and defines the adaptation of APD as a function of the heart rate. It's slope has a heterogeneous spatial distribution, which can play a crucial role in arrhythmogenesis [22], [29], [9]. The APD Restitution Curve (RC) defines the relationship between the next cycle APD and the Diastolic Interval (DI) of the previous cycle. The slope of these RCs is controlled by τ_{open} and depicts the APD heterogeneity present at multiple heart rates. APD RC for MS model is explicitly derived as [31],

$$APD_{n+1} = f(DI_n) = \tau_{close} \ln \left\{ \frac{1-(1-h_{min})e^{\frac{-DI_n}{\tau_{open}}}}{h_{min}} \right\} \tag{6}$$

where $h_{min} = 4\,(\tau_{in}/\tau_{out})$ and n is the cycle number. The maximum value of APD is also explicitly derived as,

$$g = APD_{max} = \tau_{close} \ln \left(\frac{1}{h_{min}} \right) \tag{7}$$

LV Endocardial values. As we had recordings for the paced mode with 100 bpm and a sinus rhythm rate (baseline). Therefore, for the estimation of the RC slope from APD-DI values at two rates, we assume that APD_{max} (asymptotic value of APD RC) should be approximately equal to the normal sinus rhythm APD, and the slope value is adjusted with paced mode APD. From eq 6 & eq 7, we can observe that τ_{close} and h_{min} control both APD RC and APD_{max}, hence we estimate the parameters minimising the error on them jointly. The cost function minimised is,

$$\min_{\theta} \sum_{j=1}^{N} ((f(DI_{msd}^{i,j}, \theta^i) - APD_{msd}^{i,j})^2 + (g(\theta^i) - APD_{SR_{msd}}^{i,j})^2) \tag{8}$$

with N as total number of pacing rates, i as the vertex having data (LV surface only), $\theta = [\tau_{\text{close}}, \tau_{\text{open}}]$, $APD_{SR_{msd}}$ as measured sinus rhythm APD and DI_{msd} measured from the data as $DI_{msd} = 1/f - APD_{msd}$, where f is the heart rate (in Hz).

Only APD restitution is estimated as we only have two pacing frequencies, but additional data would allow to also estimate CV restitution, as demonstrated on experimental data in [39], [40]. Parameter h_{min} is not estimated here but kept to the literature value [31] as it also controls the CV unlike τ_{close} & τ_{open}, thus disturbing the CV adjustments done before. The parameter optimisation method used here is a non-linear constrained Active-Set Algorithm, with constraints on τ_{close} & τ_{open} to be in the range of literature values [31]. Fig. 10c shows the fit of RC to data.

Minimum DI can also be computed explicitly from the estimated parameter values (Fig. 10c) as described in [31],

$$DI_{min} = \tau_{open} \ln \left(\frac{1-h_{min}}{1-h_{thr}} \right) \tag{9}$$

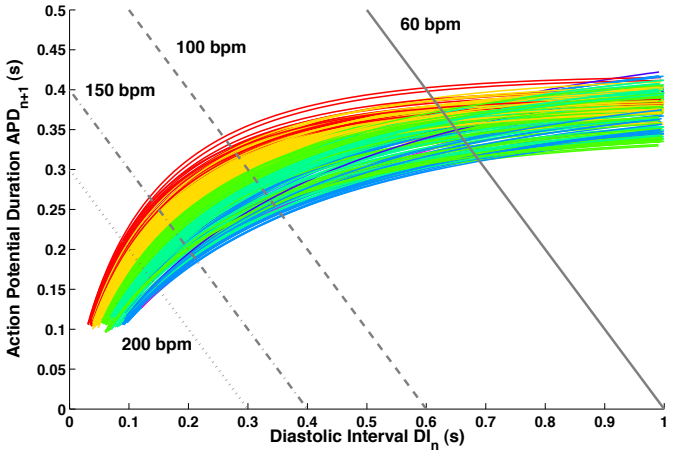

Fig. 8. Computation of local steady-state APDs for different cycle lengths from the estimated restitution curves. Red to blue colors represent steep to flat slopes.

where,

$$h_{thr} = \frac{h_{min}}{4v_{stim}(1-v_{stim})} \text{ with } v_{stim} \approx \int J_{stim}(t)dt$$

with J_{stim} as defined in eq 2.

LV & RV Myocardial values. For RV, we fix one value measured from the QT interval given through the surface ECG. To have a smooth gradation of APD restitution from epicardium to endocardium, we diffuse the τ_{close} & τ_{open} values spatially in the LV myocardium from endocardium to epicardium as in [41] (Fig. 10d).

Steady-state APDs for a pacing frequency f could then be estimated from the intersection of the line $DI_n = 1/f - APD_{n+1}$ with the personalised RCs (Fig. 8). The model personalisation times are given in Table. II.

V. Results

A. Parameter Estimation

The AC parameters estimated using the EK model, see Fig. 10a, show high conduction areas on parts of the endocardium, potentially depicting the Purkinje network extremities, and a conduction block near the scar. The coupled MS model conductivity parameters were then estimated from this AC map. The mean absolute error on

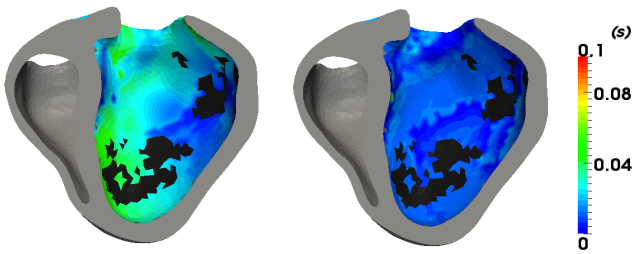

(a) (b)

Fig. 9. Maps of absolute (a) depolarisation time error and (b) APD error between simulated and measured isochrones.

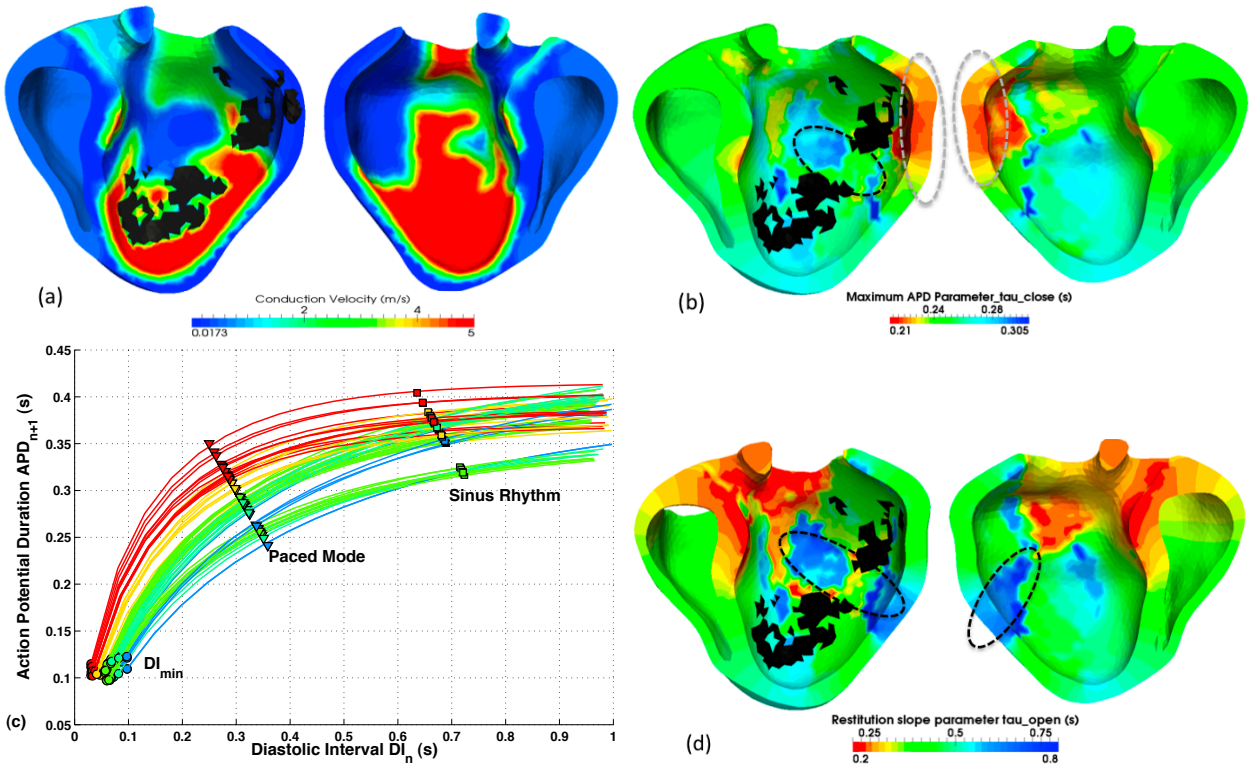

Fig. 10. Estimated parameters: (a) conduction velocity estimated from AC maps, (b) APD parameter τ_{close}, lower τ_{close} values correspond to lower measured APD (white ellipse), (c) & (d) heterogeneous APD restitution curves and APD RC parameter τ_{open} maps respectively, low τ_{open} values (red) correspond to steep RC slopes & high values (blue) correspond to flat RC slopes. Heterogeneous Minimum DI values for the restitution curves are also shown in (c)

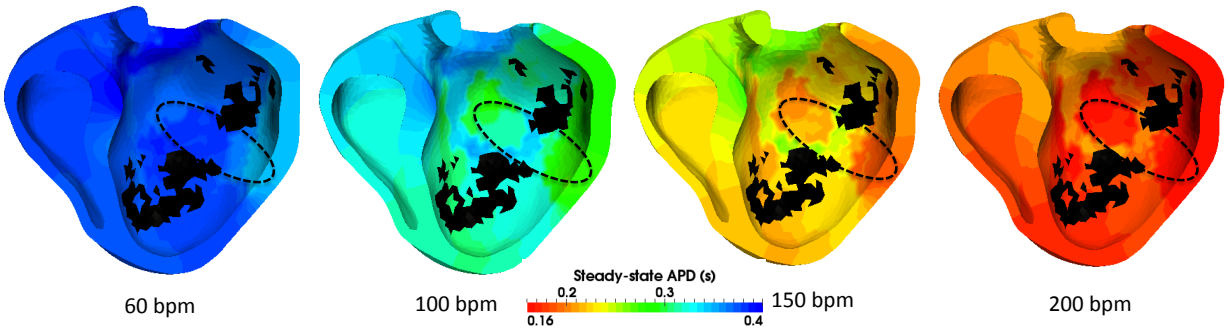

Fig. 11. Steady state values of APD for different pacing rates. Black ellipse highlights the changes in heterogeneity near the scars and isthmus.

simulated depolarisation times after personalisation was 7.1ms for the EK model and 18.5ms for the MS model ($\approx 10-14\%$ of depolarisation duration 131ms), see Fig. 6 & 9a. The mean absolute error on APD was 8.71ms ($\approx 2\%$ of APD 300ms), showing a good fit as well, see Fig. 6 & 9b.

Fig. 10b shows the heterogeneity of the steady-state APD in terms of the estimated parameter τ_{close}, as it is shorter on the free wall of the LV compared to the septum (white ellipse). Also there is a longer APD compared to the neighbours near the scar (gray zones) and the region between the two scars (isthmus) Fig. 10b (black ellipse). For APD restitution, the mean absolute error after fitting the curves was 1.13ms, showing a good fit, see Fig. 10c. The region around the scars and the isthmus were more heterogeneous for RC slope parameter τ_{open} than the rest of the LV, see Fig. 10d black ellipses. In Fig. 10d, red color (low values of τ_{open}) corresponds to steep slopes and blue color (high values of τ_{open}) corresponds to flat slopes, as shown in Fig. 10c. The color bar is also applicable to the RCs. A smooth apex-to-base gradient for APD RC can be observed in Fig. 10d. Isthmus and gray zones were seen to have high APD values with more heterogeneous RC slopes and conduction. All of these factors along with the scar geometry did play a crucial role in induction of ischemic VT as explained later.

B. Assessment of Heterogeneity Maps

Such maps reveal areas with a risk of VT (black ellipse in Fig. 11). But this is also highly dependent on the pacing location, thus in order to really assess this risk we simulate VT-Stim procedures with various pacing locations.

In order to better interpret these parameter maps, we estimated the steady-state APD maps for different pacing frequencies, see Fig. 11. We can observe that this map is quite homogeneous for slow pacing frequency (60 bpm), but its heterogeneity then increases with pacing rate (100, 150 bpm). Eventually it reaches a kind of plateau where it is then quite homogeneous (200 bpm).

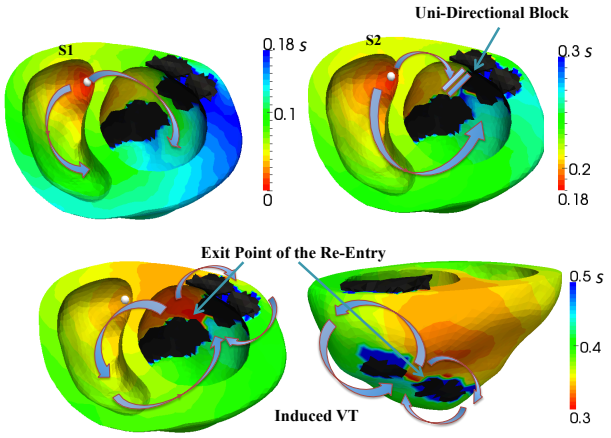

Fig. 12. DT isochrones for simulated S1-S2 VT-Stim protocol. Personalised anatomy and synthetic electrophysiology parameter set were used here with steep RC slopes and low CV in isthmus compared to flat RC slopes and high CV in the rest of myocardium. S_1 stimulus shows a normal propagation and S_2 shows a unidirectional block created in the isthmus due to APD heterogeneity. Bottom row shows DT isochrones for induced monomorphic VT.

C. Ischemic Ventricular Tachycardia Stimulation

Programmed ventricular stimulation is a clinical protocol and consists of a number of extra stimuli introduced at two ventricular sites (RV-Apex (RVA) & RV-Outflow tract (RVOT)), using various Cycle Lengths (CL), with varying coupling interval. This protocol is tested directly on the patient, without any planning, to collect information about the VT and to plan the RF ablation lines. We illustrate on Fig. 12 how such pacing can develop VT. It may be time consuming or fail, when VT is not inducible and recurrent. Here we followed a conventional VT-Stim protocol [42] with an RVA pacing site, two extra stimuli and a shortest coupling interval of 200 ms at 600 ms pacing cycle length. The induced VT specifications are given in Table. III

Synthetic Simulation. First case of simulation of this protocol *in silico* was performed on the patient's ventricular and scar geometry, but synthetic model parameter set as shown in Fig. 12, and detailed in [43].

Personalised Simulation. We then used the personalised 3D MS model of our patient data to simulate this protocol. The VT-Stim simulation using RVA & RVOT on this patient did not induce any VT. This is in agreement with the clinical data on this patient who did not have any VT episode. However we could induce VT using various other pacing sites in LV, as explained next.

D. Towards VT Risk Maps

Personalised models offer much more flexibility in the VT-Stim procedure, as the model can be paced from any location, and at any pacing rate which would not be possible in practice. We used this by running on a cluster of computers[1] series of VT-Stim procedures from many different points of the heart. This provides insights on which points of the heart could be a source of VT if paced [44]. We then obtained sustained VTs when pacing from particular locations (Fig. 13), due to the surrounding heterogeneity in restitution and conductivity (Fig. 10).

We now need to obtain clinical data on activation maps of sustained VTs in order to validate our VT simulations [44], [42]. Such maps are difficult to acquire as routine VT-Stim procedures do not include electro-anatomical mapping. We are currently planning a study where such data would be acquired. From these VT-Stim simulations we can build a VT risk map for a given patient. As an ectopic focus can be generated by ischemic cells [45], [46], thus from any location in the myocardium, building such risk maps could have an important clinical impact when taking decisions regarding defibrillator implantation and RF ablation.

VI. Discussion

A. Data Limitations

As only LV endocardial mapping data were used in this paper, the model personalisation had several limitations, few of which are: (*i*) Lack of estimation of local RV and transmural spatial distributions of conductivity and restitution properties. A global estimation of these properties was done using body surface ECG waveforms as explained in Sec. IVA & C. (*ii*) Only two heart rates were used for fitting APD RCs. Thus only two model parameters were estimated, and an assumption was made by considering the sinus rhythm APD, as a constraint on the asymptotic value of APD RCs controlled by the parameter τ_{close}, while the paced mode APD was used to adjust the RC slope controlled by the parameter τ_{open}. However, more measurements for frequencies in the slope region (region between minimum DI and maximum value of APD on APD RC) could have depicted the RC slope more accurately. (*iii*) Lack of minimum DI measurement with pacing periods reaching upto the refractory period of the myocardium. As these values can play a crucial role in the initiation and sustainability of arrhythmias. However the model had its own simulated minimum DI derived from the estimated parameters as shown in Sec. IV.C and (*iv*) Usage of Non-Contact Mapping (NCM) data and EP & MR fusion errors. Although NCM data do have an advantage of measuring temporal EP data with more spatial acquisition (surface)

[1] 64 nodes of IBM e325 dual-Opterons 246, 2Ghz

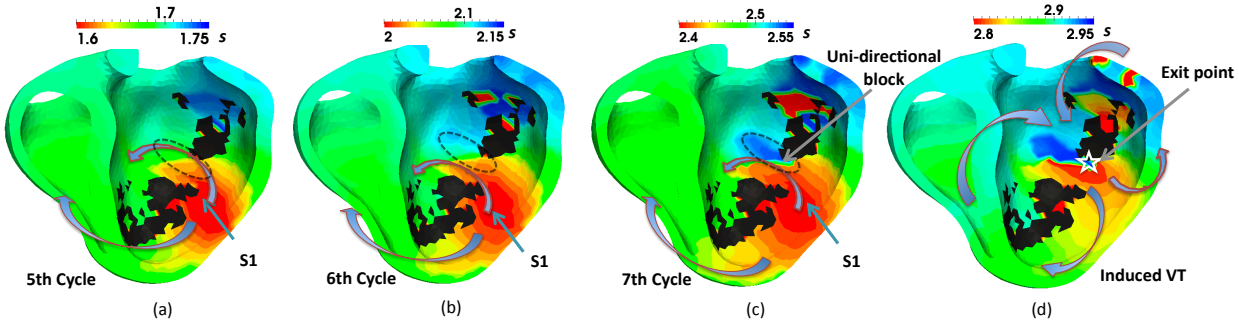

Fig. 13. †DT isochrones for simulated VT-Stim protocol for over-drive pacing using the personalised electrophysiology parameters, with pacing near the scars (shown by arrow) at 400 ms cycle length (≈ 150 bpm). (a) shows normal propagation (b) & (c) show increase in heterogeneity in conduction near the isthmus after 7 cycles due to APD and refractoriness heterogeneity (black ellipse) and (d) no pacing and induced VT of 250 ms cycle length (≈ 240 bpm) with an exit point (shown by a star).

than the contact mapping data (point), the NCM data can be challenging for local depolarisation and repolarisation time estimations. Also uncertainty on the data can be added due to the difficult registration between the ensite LV surface and the MR-derived LV surface (Fig. 4).

B. Model Simplifications

In order to have a clinical relevant model for personalisation and VT risk assessment, the MS model used had several simplifications, few of which are, (*i*) No actual purkinje network modelling. Exact locations of these purkinje network extremities are ambiguous and inextractable from the patients data, although they could play a crucial role in arrhythmogenesis [47], [46]. However, a high conductivity endocardial region was obtained, which may be inferred as depicting the underlying purkinje network with personalisation (Sec. IVA & Fig 10a). A local estimation of endocardial restitution properties (Sec. IV.C & Fig 10d) also helped potentially depict the abnormalities in the purkinje network around scars, leading to arrhythmia generation. (*ii*) Use of an atlas-based cardiac fibre model. Extraction of true *in-vivo* cardiac fibre orientations is the subject of ongoing research and including them would give more accuracy to the VT-Stim predictions and inducibility maps. Finally, orthotropic anisotropy could change the model behaviour, but acquiring patient-specific data on cardiac laminar sheets seems even more challenging.

VII. Conclusion

The proposed approach of coupled model personalisation for fast estimation of hidden parameters such as conductivity and APD restitution could enable the clinical use of cardiac electrophysiology models in the future. The parameter estimation algorithm is used on clinical interventional data and the obtained results are very encouraging. The estimated conductivity and APD restitution parameters are able to distinguish between the healthy areas and the pathological ones (scar and isthmus). Then a clinical VT-Stim protocol was simulated on the personalised MS model in order to assess the risk of VT and fibrillation for a patient-specific case. This opens up possibilities of evaluating the role of patient-specific models in the clinics to provide aid in treatment and planning of RF ablation. In the future, we need to validate the personalised model predictions with mapping data for arrhythmias and integrate the simulation of RF ablation into a first cohort of clinical cases.

†A video on personalised induced VT simulation is available as a supplementary material. A few snapshots of the same are presented in Fig. 14 demonstrating the re-entry wave.

TABLE I
Electrophysiology Model Parameters

EK Model		MS Model	
Parameter	Value	Parameter	Value
d_{EK}	estimated	d_{MS}	coupled
c_0	2.5	τ_{in}	0.003 s
τ	0.003 s	τ_{out}	0.06 s
		τ_{open}	estimated
		τ_{close}	estimated
		u_{gate}	0.13
		v_{stim}	0.2

Acknowledgment

This research received funding from the European Community's Seventh Framework Programme (FP7/2007-2013) under grant agreement n 224495 (euHeart project).

Appendix

The MS model was personalised on a volumetric tetrahedral mesh of a 4 valve bi-ventricular anatomy with a Mean Edge Length (MEL) of 1.0 *mm* and 65547 number of tetrahedrons. The model parameters, simulation, personalisation and VT induction specifications are detailed in TABLE I, II & III respectively.

References

[1] E. Aliot, W. Stevenson, and J. Almendral-Garrote, "EHRA/HRS expert consensus on catheter ablation of ventricular arrhythmias," *Europace*, vol. 11, pp. 771–817, 2009.

[2] W. Stevenson, H. Khan, P. Sager, S. LA., H. Middlekauff, P. Natterson, and I. Wiener, "Identification of reentry circuit sites during catheter mapping and radiofrequency ablation of ventricular tachycardia late after myocardial infarction," *Circulation*, vol. 88, pp. 1647–1670, 1993.

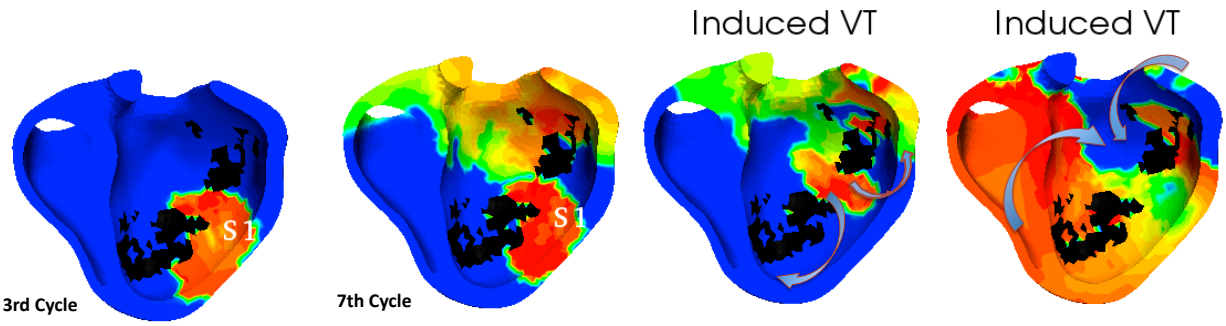

Fig. 14. Induced VT in the personalised model. At the 7th cycle of the pacing overdrive, some areas in the isthmus have the previous S1 wave-back touching the wave-front of the next S1 wave, thus creating an uni-directional block. A monomorphic sustained VT then develops.

TABLE II
MODEL SIMULATION & PERSONALISATION SPECIFICATIONS

	EK Model	MS Model
Spatial Integration	FMM	FEM
Spatial step size (MEL) $\delta(x)$	1.0 mm	1.0 mm
Temporal Integration	-	MCNAB
Temporal step size $\delta(t)$	-	0.03 ms
Computational Time (CT) per $10\delta(t)$	-	$\approx$ 1 s
CT for 1 cycle dep phase (150 ms)	$\approx$ 1-2 s	$\approx$ 500 s
AC Estimation Time	$\approx$ 30-40 min	-
Coupled conductivity Estimation Time	-	$\approx$ 1 s
Restitution Estimation Time	-	$\approx$ 2-5 min

TABLE III
INDUCED VT SPECIFICATIONS

VT-stim protocol	Over-drive pacing
VT-stim location	LV endocardium - apex
VT-stim pacing frequency	150 bpm
VT-stim pacing duration	5 s
Induced VT type	sustained monomorphic VT
Induced VT frequency	240 bpm

[3] F. H. Fenton and E. M. Cherry, "Models of cardiac cell," *Scholarpedia*, vol. 3, no. 8, p. 1868, 2008.

[4] C. Luo and Y. Rudy, "A model of the ventricular cardiac action potential. depolarization, repolarization, and their interaction," *Circulation Research*, vol. 68, no. 6, p. 1501, 1991.

[5] D. Noble, A. Varghese, P. Kohl, and P. Noble, "Improved guinea-pig ventricular cell model incorporating a diadic space, IKr and IKs, and length-and tension-dependent processes." *The Canadian journal of cardiology*, vol. 14, no. 1, p. 123, 1998.

[6] K. Ten Tusscher, D. Noble, P. Noble, and A. Panfilov, "A model for human ventricular tissue," *American Journal of Physiology-Heart and Circulatory Physiology*, vol. 286, no. 4, p. H1573, 2004.

[7] M. Fink, S. A. Niederer, E. M. Cherry, F. H. Fenton, J. T. Koivumki, G. Seemann, R. Thul, H. Zhang, F. B. Sachse, D. Beard, E. J. Crampin, and N. P. Smith, "Cardiac cell modelling: Observations from the heart of the cardiac physiome project," *Progress in Biophysics and Molecular Biology*, vol. 104, no. 1-3, pp. 2 – 21, 2011, cardiac Physiome project: Mathematical and Modelling Foundations.

[8] F. Sachse, *Computational cardiology: modeling of anatomy, electrophysiology, and mechanics*. Springer-Verlag New York Inc, 2004.

[9] R. Clayton, O. Bernus, E. Cherry, H. Dierckx, F. Fenton, L. Mirabella, A. Panfilov, F. Sachse, G. Seemann, and H. Zhang, "Models of cardiac tissue electrophysiology: Progress, challenges and open questions," *Progress in Biophysics and Molecular Biology*, vol. 104, no. 1-3, pp. 22 – 48, 2011, cardiac Physiome project: Mathematical and Modelling Foundations.

[10] O. Bernus, R. Wilders, C. Zemlin, H. Verschelde, and A. Panfilov, "A computationally efficient electrophysiological model of human ventricular cells," *American Journal of Physiology-Heart and Circulatory Physiology*, vol. 282, no. 6, p. H2296, 2002.

[11] A. Bueno-Orovio, E. Cherry, and F. Fenton, "Minimal model for human ventricular action potentials in tissue," *Journal of theoretical biology*, vol. 253, no. 3, pp. 544–560, 2008.

[12] R. Fitzhugh, "Impulses and physiological states in theoretical models of nerve membrane," *Biophysical Journal*, vol. 1, no. 6, pp. 445–466, 1961.

[13] R. R. Aliev and A. V. Panfilov, "A simple two-variable model of cardiac excitation," *Chaos, Solitons & Fractals*, vol. 7, no. 3, pp. 293–301, 1996.

[14] J. Keener and J. Sneyd, *Mathematical physiology: Cellular physiology*. Springer Verlag, 2009.

[15] P. Colli Franzone, L. Guerri, and S. Rovida, "Wavefront propagation in an activation model of the anisotropic cardiac tissue: asymptotic analysis and numerical simulations," *Journal of mathematical biology*, vol. 28, no. 2, pp. 121–176, 1990.

[16] M. Sermesant, E. Konukoglu, H. Delingette, Y. Coudiere, P. Chinchapatnam, K. Rhode, R. Razavi, and N. Ayache, "An anisotropic multi-front fast marching method for real-time simulation of cardiac electrophysiology," vol. 4466 of LNCS. Springer, 2007, pp. 160–169.

[17] P. Chinchapatnam, K. Rhode, M. Ginks, C. Rinaldi, P. Lambiase, R. Razavi, S. Arridge, and M. Sermesant, "Model-based imaging of cardiac apparent conductivity and local conduction velocity for diagnosis and planning of therapy," *Medical Imaging, IEEE Transactions on*, vol. 27, no. 11, pp. 1631–1642, 2008.

[18] M. Courtemanche and A. T. Winfree, "Re-entrant rotating waves in a beeler–reuter based model of two-dimensional cardiac electrical activity," *Int. J. Bifurcation & Chaos*, no. 1, pp. 431–444, 1991.

[19] M. Watanabe, F. Fenton, S. Evans, H. Hastings, and A. Karma, "Mechanisms for discordant alternans," *Journal of Cardiovascular Electrophysiology*, vol. 12, no. 2, pp. 196–206, 2001.

[20] A. Panfilov and J. Keener, "Re-entry in an anatomical model of the heart," *Chaos, Solitons & Fractals*, vol. 5, no. 3-4, pp. 681–689, 1995.

[21] J. Jalife and R. Gray, "Drifting vortices of electrical waves underlie ventricular fibrillation in the rabbit heart," *Acta Physiologica Scandinavica*, vol. 157, no. 2, pp. 123–132, 1996.

[22] E. Cherry and F. Fenton, "Suppression of alternans and conduction blocks despite steep APD restitution: electrotonic, memory, and conduction velocity restitution effects," *American Journal of Physiology- Heart and Circulatory Physiology*, vol. 286, no. 6, p. H2332, 2004.

[23] C. Clancy and Y. Rudy, "Linking a genetic defect to its cellular phenotype in a cardiac arrhythmia," *Biol*, vol. 9, pp. 295–305, 1995.

[24] N. A. Trayanova and B. M. Tice, "Integrative computational models of cardiac arrhythmias - simulating the structurally realistic heart," *Drug Discovery Today: Disease Models*, vol. 6, no. 3, pp. 85 – 91, 2009, arrhythmia.

[25] M. Killeen, I. Sabir, A. Grace, and C. Huang, "Dispersions of repolarization and ventricular arrhythmogenesis: Lessons from animal models," *Progress in biophysics and molecular biology*, vol. 98, no. 2-3, pp. 219–229, 2008.

[26] A. Yue, M. Franz, P. Roberts, and J. Morgan, "Global endocardial electrical restitution in human right and left ventricles determined by noncontact mapping," *Journal of the American College of Cardiology*, vol. 46, no. 6, p. 1067, 2005.

[27] H. Arevalo, B. Rodriguez, and N. Trayanova, "Arrhythmogenesis in the heart: Multiscale modeling of the effects of defibrillation shocks and the role of electrophysiological heterogeneity," *Chaos: An Interdisciplinary Journal of Nonlinear Science*, vol. 17, p. 015103, 2007.

[28] I. Banville and R. Gray, "Effect of action potential duration and conduction velocity restitution and their spatial dispersion on alternans and the stability of arrhythmias," *Journal of cardiovascular electrophysiology*, vol. 13, no. 11, pp. 1141–1149, 2002.

[29] M. Nash, C. Bradley, P. Sutton, R. Clayton, P. Kallis, M. Hayward, D. Paterson, and P. Taggart, "Whole heart action potential duration restitution properties in cardiac patients: a combined clinical and modelling study," *Experimental physiology*, vol. 91, no. 2, p. 339, 2006.

[30] M. Sermesant, Y. Coudière, V. Moreau-Villéger, K. Rhode, D. Hill, and R. Ravazi, "A fast-marching approach to cardiac electrophysiology simulation for XMR interventional imaging," in *Proceedings of MICCAI'05*, ser. LNCS, vol. 3750. Springer, 2005, pp. 607–615.

[31] C. Mitchell and D. Schaeffer, "A two-current model for the dynamics of cardiac membrane," *Bulletin of mathematical biology*, vol. 65, no. 5, pp. 767–793, 2003.

[32] K. Rhode, M. Sermesant, D. Brogan, S. Hegde, J. Hipwell, P. Lambiase, E. Rosenthal, C. Bucknall, S. Qureshi, J. Gill, R. Razavi, and D. Hill, "A system for real-time XMR guided cardiovascular intervention," *IEEE Transactions on Medical Imaging*, vol. 24, no. 11, pp. 1428–1440, 2005.

[33] J. Peyrat, M. Sermesant, X. Pennec, H. Delingette, C. Xu, E. McVeigh, and N. Ayache, "A computational framework for the statistical analysis of cardiac diffusion tensors: Application to a small database of canine hearts," *Medical Imaging, IEEE Transactions on*, vol. 26, no. 11, pp. 1500–1514, 2007.

[34] R. Coronel, F. J. Wilms-Schopman, J. R. de Groot, M. J. Janse, F. J. van Capelle, and J. M. de Bakker, "Laplacian electrograms and the interpretation of complex ventricular activation patterns during ventricular fibrillation," *J Cardiovasc Electrophysiol*, vol. 11, no. 10, pp. 1119–1128, Oct 2000.

[35] M. Potse, A. Vinet, T. Opthof, and R. Coronel, "Validation of a simple model for the morphology of the t wave in unipolar electrograms," *American Journal of Physiology- Heart and Circulatory Physiology*, vol. 297, no. 2, p. H792, 2009.

[36] K. Tomlinson, P. Hunter, and A. Pullan, "A finite element method for an eikonal equation model of myocardial excitation wavefront propagation," *SIAM Journal on Applied Mathematics*, vol. 63, no. 1, pp. 324–350, 2002.

[37] F. Fenton and A. Karma, "Vortex dynamics in three-dimensional continuous myocardium with fiber rotation: filament instability and fibrillation," *Chaos*, vol. 8, no. 1, pp. 20–47, 1998.

[38] J. Relan, M. Sermesant, H. Delingette, M. Pop, G. Wright, and N. Ayache, "Quantitative comparison of two cardiac electrophysiology models using personalisation to optical and mr data," in *Biomedical Imaging: From Nano to Macro, 2009. ISBI'09. IEEE International Symposium on.* IEEE, 2009, pp. 1027–1030.

[39] J. Relan, M. Pop, H. Delingette, G. Wright, N. Ayache, and M. Sermesant, "Personalisation of a cardiac electrophysiology model using optical mapping and mri for prediction of changes with pacing." *Biomedical Engineering, IEEE Transactions on*, 2011.

[40] ——, "Personalisation of a 3D cardiac electrophysiology model for ventricular myocardium using optical mapping and MRI," in *MICCAI Workshop (STACOM) and (CESC'10)*, ser. LNCS, vol. 6364. Springer, 2010.

[41] R. Keldermann, K. Ten Tusscher, M. Nash, R. Hren, P. Taggart, and A. Panfilov, "Effect of heterogeneous APD restitution on VF organization in a model of the human ventricles," *American Journal of Physiology- Heart and Circulatory Physiology*, vol. 294, no. 2, p. H764, 2008.

[42] F. Morady, A. Kadish, M. De Buitleir, W. Kou, H. Calkins, S. Schmaltz, S. Rosenheck, and J. Sousa, "Prospective comparison of a conventional and an accelerated protocol for programmed ventricular stimulation in patients with coronary artery disease," *Circulation*, vol. 83, no. 3, p. 764, 1991.

[43] J. Relan, P. Chinchapatnam, M. Sermesant, K. Rhode, H. Delingette, R. Razavi, and N. Ayache, "Coupled personalisation of electrophysiology models for simulation of induced ischemic ventricular tachycardia," in *Medical Image Computing and Computer-Assisted Intervention–MICCAI 2010*, vol. 6362 of LNCS. Springer, 2010, pp. 420–428.

[44] H. Wellens, P. Brugada, and W. Stevenson, "Programmed electrical stimulation of the heart in patients with life-threatening ventricular arrhythmias: what is the significance of induced arrhythmias and what is the correct stimulation protocol?" *Circulation*, vol. 72, no. 1, p. 1, 1985.

[45] F. Bogun, T. Crawford, N. Chalfoun, M. Kuhne, J. Sarrazin, D. Wells, E. Good, K. Jongnarangsin, H. Oral, A. Chugh *et al.*, "Relationship of frequent postinfarction premature ventricular complexes to the reentry circuit of scar-related ventricular tachycardia," *Heart Rhythm*, vol. 5, no. 3, pp. 367–374, 2008.

[46] L. Szumowski, P. Sanders, F. Walczak, M. Hocini, P. Jais, R. Kepski, E. Szufladowicz, P. Urbanek, P. Derejko, R. Bodalski *et al.*, "Mapping and ablation of polymorphic ventricular tachycardia after myocardial infarction," *Journal of the American College of Cardiology*, vol. 44, no. 8, p. 1700, 2004.

[47] F. Bogun, E. Good, S. Reich, D. Elmouchi, P. Igic, D. Tschopp, S. Dey, A. Wimmer, K. Jongnarangsin, H. Oral *et al.*, "Role of Purkinje fibers in post-infarction ventricular tachycardia," *Journal of the American College of Cardiology*, vol. 48, no. 12, p. 2500, 2006.